Relationship between sea surface temperature, vertical dynamics, and the vertical distribution of atmospheric water vapor inferred from TOVS observations

Jean-pierre Chaboureau, Alain Chédin, Noëlle A Scott

JOURNAL OF GEOPHYSICAL RESEARCH, VOL. 103, NO. D18, PAGES 23,173–23,180, SEPTEMBER 27, 1998

Relationship between sea surface temperature, vertical dynamics, and the vertical distribution of atmospheric water vapor inferred from TOVS observations

Jean-Pierre Chaboureau,[1] Alain Chédin, and Noëlle A. Scott
Laboratoire de Météorologie Dynamique du CNRS, École Polytechnique, Palaiseau, France

Abstract. With the aim of better understanding the respective role of sea surface temperature (SST) and vertical dynamics on the vertical distribution of atmospheric water vapor, particularly in the tropics, global scale observations from NOAA 10, covering a 31-month period, have been processed using the improved initialization inversion ((3I) [*Chédin and Scott*, 1984]) retrieval method and interpreted in terms of tropospheric layered water vapor contents. The method of analysis uses the power law, which expresses the specific humidity q at pressure p as a function of their values at the surface, q_0 and p_0; $q = q_0(p/p_0)^{\lambda}$. This description is applied independently to three layers giving three values of λ: λ_1 for surface–700 hPa, λ_2 for 700–500 hPa, and λ_3 for 500–300 hPa. It is shown that λ_2 is a good indicator of the large-scale vertical dynamics and gives results equivalent to those obtained using the vertical velocity at 500 hPa issued from a model. Consequently, the role of enhanced upward motion with increased SST for the "super greenhouse effect" situations is confirmed as well as the contribution of externally forced subsidence on the suppression of the deep convection for cases where SSTs exceed about 303 K. In addition, the influence of SST on the vertical distribution of water vapor is analyzed together with the large-scale vertical dynamics contribution. The results show that the rate of change of water vapor content in the 700- to 500-hPa and 500- to 300-hPa layers with respect to SST increases with decreasing rate of change of λ_2 with respect to SST, that is, with increasing rate of change of upward vertical dynamics with respect to SST.

1. Introduction

Water vapor, owing to its abundance, is the most important greenhouse gas, and its interaction within the atmosphere plays a fundamental role in regulating Earth's climate at all timescales. Therefore the water vapor feedback, in which surface temperatures lead to increased water vapor concentrations hence amplifying greenhouse trapping, is considered as an important scheme of warming in the global climate change simulations of general circulation models [*Cess et al.*, 1990]. Using observations, *Raval and Ramanathan* [1989] showed the strong positive correlation between greenhouse effect and sea surface temperature (SST). They attributed this increase of greenhouse effect to increasing total water vapor content, and *Stephens and Greenwald* [1991] confirmed the strong correlation between total water vapor content and greenhouse effect. However, *Lindzen* [1990] suggested that, although rapid mixing in the lower atmosphere should increase the specific humidity as SST increases, stronger convective activity could lead to decreased specific humidity in the upper troposphere, resulting in a potential negative feedback. This latter argument has stirred much controversy regarding the water vapor feedback and associated processes limiting the rise in SST [*Ramanathan and Collins*, 1991; *Rind et al.*, 1991; *Fu et al.*, 1992; *Wallace*, 1992; *Inamdar and Ramanathan*, 1994].

Thus the role of the convection and the associated vertical motions have been pinpointed to explain discontinuities in the mean spatiotemporal relationships between the SST and water vapor, clouds, or radiation. In a range of SST greater than about 298 K, *Raval and Ramanathan* [1989] found situations where the increase of the greenhouse trapping with SST exceeds the rate of increase in infrared surface emission with SST. *Hallberg and Inamdar* [1993] have suggested that large-scale dynamical processes are involved in this phenomenon, often referred to as the "super greenhouse effect." Using both model analyses and satellite observations, *Bony et al.* [1997] have shown that these situations are linked to an enhanced large-scale atmospheric rising motion with increasing SST. For monthly average SST values in excess of about 302.5 K, only conditions of diminished convection tend to occur [*Waliser et al.*, 1993]. *Chahine* [1995] also observed that the distribution of atmospheric moisture reaches a maximum value when the daily surface temperature approaches 304 ± 1 K. *Waliser and Graham* [1993] suggest the deep convection is suppressed by externally forced subsidence, which is also observed by *Bony et al.* [1997].

To investigate the role of the vertical dynamics, here we use geophysical variables (temperature profiles, layered water vapor contents, and cloud and surface parameters) only derived from satellite observations. The radiative information comes from the TIROS-N operational vertical sounder (TOVS), aboard the National Oceanic and Atmospheric Administration (NOAA) series of polar satellites, operational since 1979. Within the framework of international projects (NOAA/NASA Pathfinder and Global Energy and Water Cycle Experiment (GEWEX) Water Vapor Project, a global data set has

[1]Now at Department of Meteorology, University of Reading, England.

Paper number 98JD02019.
0148-0227/98/98JD-02019$09.00

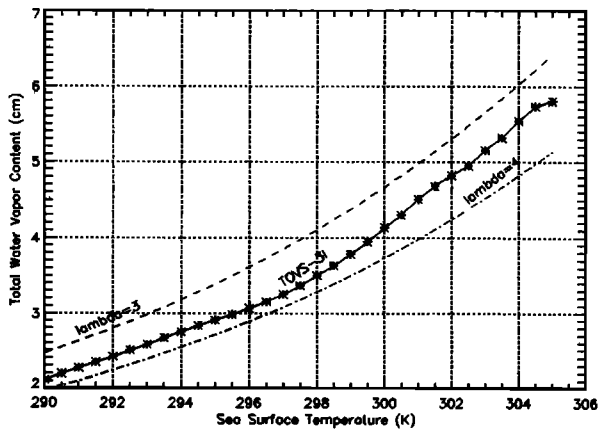

Figure 1. The value w_{tot} versus sea surface temperature (SST) observed by TOVS improved initialization inversion (3I) (over oceans for which SSTs are greater than 290 K, values averaged from April 1987 to March 1989) and computed using equation (1) for two values of λ.

been created from NOAA 10 TOVS observations over a 31-month benchmark period (April 1987 to October 1989), using the improved initialization inversion (3I) algorithm [*Chédin and Scott*, 1984; *Chédin et al.*, 1985].

To infer the large-scale vertical dynamics, an original method has been developed from the power law. The latter depicts approximately the distribution of water vapor on the vertical. A specific indicator of the large-scale vertical dynamics is then defined and validated using, in particular, the retrieved cloud distribution. The method permits us to express the relationship between the water vapor vertical structure, the SST, and this index of large-scale vertical motions.

Section 2 presents the satellite data and the associated retrieval method. Section 3 describes the method to identify the vertical dynamics indicator. Section 4 establishes the relationship between the water vapor distribution, the SST, and the vertical dynamics. The conclusions are given in section 5.

2. TOVS Observations and the 3I Method

TOVS consists of three passive vertical sounding instruments [*Smith et al.*, 1979]: the high-resolution infrared radiation sounder (HIRS-2), a radiometer with 19 channels in the infrared band and one in the visible band; the microwave sounding unit (MSU), a microwave sounder with four channels in the vicinity of 55 GHz; and the stratospheric sounding unit, a pressure-modulated infrared radiometer with three channels near 15 μm. To retrieve atmospheric temperature and humidity fields with the 3I algorithm, only HIRS and MSU data are used. The inversion algorithm 3I is a physicostatistical method relying on pattern recognition. It determines the following parameters: air mass type, temperature profiles (from the surface to 10 hPa), cloud heights (amounts and types), surface parameters (temperature and emissivity), and water vapor contents in four layers (surface–850, 850–700, 700–500, and 500–300 hPa). For a complete description of the method the reader is referred to *Chédin and Scott* [1984] and *Chédin et al.* [1985]. Significant improvements have been brought to the method more recently by *Achard* [1991], *Escobar-Munoz* [1993], *Stubenrauch et al.* [1996], and *Chevallier et al.* [1998]. Also, the water vapor retrieval scheme has been modified and improved. It is based upon a neural network approach, directly coupling satellite observations to water vapor contents. Cross comparisons with a wide variety of independent observations (in situ measurements, other satellite retrievals, and analyses) have been conducted to fully evaluate the method [*Chaboureau et al.*, 1998].

All variables are retrieved at a spatial resolution of 100 km by 100 km. In the framework of the NOAA/NASA Pathfinder project, statistics have been calculated to produce daily, pentad (5 days), and monthly average parameters onto a 1° longitude by 1° latitude grid. A global data set of geophysical variables (temperature profiles, water vapor contents, and cloud and surface parameters) has been created over a 31-month benchmark period (April 1987 to October 1989) from NOAA 10 observations. The present study is limited to the tropical band (±30° latitude) for the 2-year period, April 1987 to March 1989, and uses monthly averages. This time period contains the dry-monsoon part of El Niño 1986–1987 and covers the La Niña event of 1988.

3. Distribution of Atmospheric Humidity and Large-Scale Vertical Dynamics

3.1. Water Vapor and the Power Law

The mean decrease of humidity with increasing altitude may be approximately described by a power law:

$$q = q_0(p/p_0)^{\lambda}, \tag{1}$$

where q is the specific humidity at pressure p, q_0 and p_0 are the respective surface values, and λ is the power factor [*Smith*, 1966]. The value λ is the ratio of the atmospheric scale height to the specific humidity scale height. If we take 7 km for a typical value of atmospheric scale height and 2 km for the specific humidity scale height, then a typical value of λ is 3.5 [*Stephens*, 1990]. The smaller λ is, the larger is the humidity in altitude.

By integrating this relation from the surface to the top of the atmosphere and by using the approximate Clausius-Clapeyron relation,

$$e^*(T) = 17{,}044 \exp[a(T - 288)], \tag{2}$$

where $e^*(T)$ is the saturation partial pressure for the temperature T and $a = 0.064\ \mathrm{K}^{-1}$ [*Stephens*, 1990], the total water vapor content (in centimeters) w_{tot} can be written as

$$w_{tot} = 10{,}82\left(\frac{r_0}{1+\lambda}\right) \exp[a(\mathrm{SST} - 288)]. \tag{3}$$

SST is the sea surface temperature, and r_0 is the relative humidity at the surface, generally considered as not too variable, around a mean value of 75% [*Peixoto and Oort*, 1992]. Equation (3) expresses the linear relationship between $\log w_{tot}$ and the SST relation established using satellite observations by *Raval and Ramanathan* [1989].

Figure 1 presents (3) for values of λ equal to 3 and 4 and with r_0 fixed at 75%. TOVS-3I observations of the mean total water vapor content over ocean, averaged from April 1987 to March 1989, are shown on Figure 1 in function of the SST. This observed relation between total water vapor content and SST approximately follows (3) for values of λ between 3 and 4.

Using (3), we can compute λ knowing the SST and w_{tot}. Earlier results from *Prabhakara et al.* [1979] and *Stephens* [1990] show that values of λ smaller than 3.5 suggest moisture

convergence and/or moist air advection, and values of λ greater than 3.5 indicate the influence of subsidence or dry air advection.

3.2. Vertical Variation of the Power Factor λ

This approach may be refined by observing the vertical structure of water vapor rather than using w_{tot}. It follows from the integration of (1) that the ratio of w_{par}, water vapor content between the pressure levels p_{sup} and p_{inf}, to w_{tot}, total water vapor content, is

$$\frac{w_{par}}{w_{tot}} = \left(\frac{p_{sup}}{p_0}\right)^{\lambda_i+1} - \left(\frac{p_{inf}}{p_0}\right)^{\lambda_i+1}, \quad (4)$$

where λ_i applies to the layer (p_{inf}; p_{sup}). The values of λ_i for three layers of the troposphere have been computed: λ_1 associated to the surface to 700-hPa layer, λ_2 associated to the 700- to 500-hPa layer, and λ_3 associated to the 500- to 300-hPa layer. We can expect that λ_i smaller than 3.5 indicates moisture convergence and/or moist air advection in the layer i, while values of λ_i greater than 3.5 indicate the influence of subsidence or dry air advection.

Figure 2 presents the geographical distribution of each λ_i for the 2-year period (from April 1987 to March 1989) over the tropical oceans. The value λ_1 varies generally between 2.5 and 4.5. The subsidence regions westward of the continents are characterized by values of λ_1 greater than 3.5, while values less than 3.5 are observed in the equatorial regions in the vicinity of the Intertropical Convergence Zone (ITCZ). The geographical distribution of λ_1 is similar to that of λ (not shown), because the 1000- to 700-hPa water vapor content mostly compounds at least two thirds of the total content. The structure of λ_3 is completely different from that of λ_1, with small variations and less contrast.

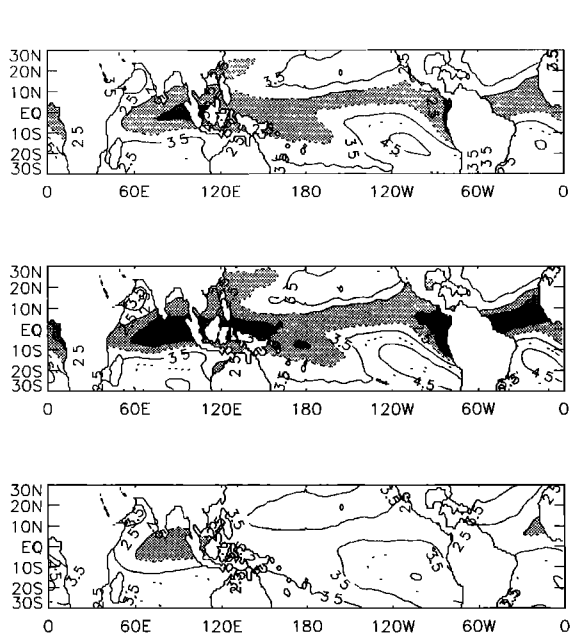

Figure 2. Geographical distribution of each λ_i for the 2-year period (from April 1987 to March 1989) over the tropical oceans. (a) The value λ_1 is associated to the surface- to 700-hPa layer, (b) λ_2 is associated to the 700- to 500-hPa layer, and (c) λ_3 is associated to the 500- to 300-hPa layer. Contour interval is 0.5, and values between 2.5 and 3 (less than 2.5) are shaded in light (dark) gray.

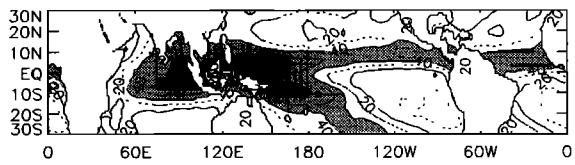

Figure 3. Geographical distribution of the 2-year mean (from April 1987 to March 1989) of frequency of occurrence of high clouds per month (FOHCM) in percent over the tropical oceans. Contour interval is 10%, and values between 40 and 60% (over 60%) are shaded in light (dark) gray.

Among the λ_i, λ_2 shows structures similar to λ_1 but with a more pronounced variability. This more contrasted behavior results from a more important influence of the large-scale vertical dynamics as shown now. To assess this affirmation, we use one of the signatures of such an influence: the high-level clouds (for which top pressure is less than 440 hPa), which include deep convective clouds associated with an upward motion. More precisely, we compute the frequency of occurrence of high clouds per month (FOHCM). Figure 3 presents the geographical distribution of the 2-year mean (from April 1987 to March 1989) of FOHCM over the tropical oceans. Maxima occur in a well-defined band over the tropical oceans, delineating the ITCZ, with broader regions of maxima over the "warm pool," the known convective region of the western Pacific. So a large amount of FOHCM implies the occurrence of upward motion.

Moreover, it has been shown that SSTs in excess of around 300 K are required for large-scale deep convection to occur [*Gadgil et al.*, 1984; *Graham and Barnett*, 1987]. *Raval and Ramanathan* [1989] found a similar SST threshold at 298 K. Figure 4 presents the geographical distribution of the 2-year mean (from April 1987 to March 1989) of SST over the tropical oceans. Regions where SSTs are greater than 300 K correspond approximately to areas where FOHCM is maximum, although it is not the case everywhere. Figure 5 illustrates the threshold associated with the presence of deep convection and then of large-scale vertical dynamics. It presents the 2-year mean of FOHCM versus SST (SST ≥ 290 K) for intervals of 0.5 K over tropical oceans. Up to 298 K, FOHCM varies weakly around 25%. From 298 K, FOHCM increases with SST up to a value of 75% near 304 K, consistent with the studies cited above. Over 304 K, FOHCM decreases in agreement with other studies but with a critical SST equal to 302–303 K for *Waliser et al.* [1993] and *Waliser and Graham* [1993] and equal to 304 K for *Chahine* [1995]. SST values in the range 299–304 K and FOHCM values in the range 30–75% are thus good indicators of large-scale vertical dynamics.

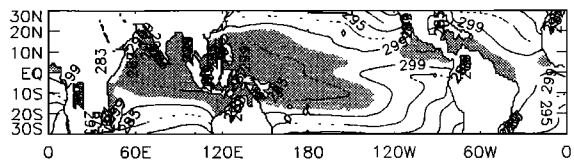

Figure 4. Geographical distribution of the 2-year mean (from April 1987 to March 1989) of SST in kelvins over the tropical oceans. Contour interval is 2 K, and values over 300 K are shaded in gray.

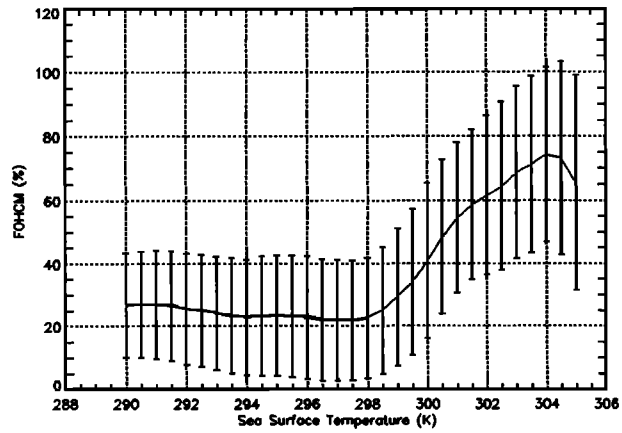

Figure 5. Monthly values of FOHCM in percent for each SST interval of 0.5 K over oceans for which SSTs are greater than 290 K from April 1987 to March 1989. Vertical bars represent plus or minus 1 standard deviation around the 2-year mean.

Figure 6 presents the variation of λ_2 versus SST (SST $\geq$ 290 K) and FOHCM, over oceans from April 1987 to March 1989. The most important feature is the anticorrelation between FOCHM and λ_2 up to 80% of FOHCM. As λ_2 decreases, FOCHM increases, showing enhanced deep convection (upward motions); the link between λ_2 and large-scale vertical dynamics associated to deep convection is straightforward. Consistently, within the range 299–303 K for SST, which is the required range for deep convection appearance, λ_2 also rapidly decreases from 3.5 to 2.5. Outside these ranges, when FOCHM increases from 0 to 20%, λ_2 decreases from 4.2 to 3.5; both small values of FOCHM and large values of λ_2 highlight the subsidence and/or dry air advection (see Figures 2b and 3). Values of λ_2 greater than 3.5 for SSTs less than 299 K also indicate the occurrence of the subsidence. Beyond 303 K for SST or 80% for FOHCM the increase of λ_2 is clearly associated with convection decrease.

4. Temporal Variations of Water Vapor, SST, and Vertical Dynamics

With λ_2 as a specific indicator of the large-scale vertical dynamics, we are now able to clarify the competitive role of dynamics and SST on the global distribution of water vapor in the atmosphere.

4.1. Geographical Distribution of the Temporal Relative Variations of SST and Vertical Dynamics

We first study the geographical distribution of the temporal variations of SST and vertical dynamics. Relative changes of vertical dynamics with respect to SST may be described by the ratio of $\Delta\lambda_2$, variation of the indicator of vertical dynamics around its annual mean, to ΔSST, variation of the SST around its annual mean. First, at each grid point, seasonal variations of each of the three variables (water vapor content, SST, and λ_2) are computed by subtracting the annual average from April 1987 to March 1988 (from April 1988 to March 1989) from monthly means from April 1987 to March 1988 (from April 1988 to March 1989). Similarly, interannual variations of the same considered variables are calculated by substracting the monthly means (e.g., July 1987) from seasonal means (e.g., July 1987–1988 mean). So I_c, the index of change of λ_2 with respect to SST, is defined as

$$I_c = (\Delta\lambda_2)/(\Delta\text{SST}) \quad (5)$$

and is computed only if ΔSST > 0.01 K to avoid unstable values for I_c. Three modes may then be defined as follows: (1) Mode 1 is $I_c < -0.2$ K^{-1}. The SST increase goes with a λ_2 decrease, for example, ascending movement increase. In particular, it should include cases driven by the mechanism of deep convection. (2) Mode 2 is $I_c > 0.2$ K^{-1}. The SST increase goes with a λ_2 increase, for example, ascending movement decrease. The change of λ_2 cannot be explained by a local SST change and thus should imply a remote forcing of the atmosphere (e.g., the large-scale subsidence). (3) Mode 3 is -0.2 K$^{-1} < I_c < 0.2$ K^{-1}. There is no (or weak) correlation between SST and vertical dynamics. Note the choice of 0.2 K^{-1} as the threshold is not critical for the following.

Figure 7 shows the geographical distribution of the occurrence (in percent) of the three different modes for the seasonal variations. Mode 1 is mainly located between 10° and 20° latitude. It corresponds to the seasonal migration of the verti-

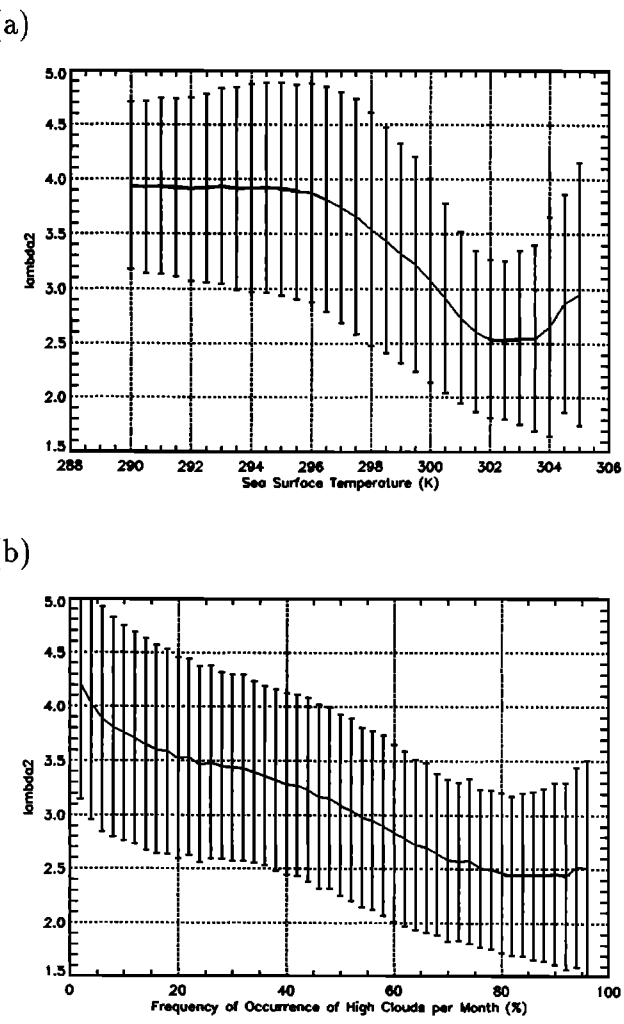

Figure 6. Monthly averaged values of λ_2 (a) for each SST interval of 0.5 K and (b) for each FOCHM interval of 2% over oceans for which SSTs are $\geq$ 290 K from April 1987 to March 1989. Vertical bars represent plus or minus 1 standard deviation around the 2-year mean.

cal branches of the Hadley circulation. These regions which show large occurrence of mode 1 are located in the vicinity of the 298- to 300-K isotherm (Figure 4), where the presence of deep convection has already been emphasized (section 3). Thus it highlights the cooperative action of a simultaneous increase of SST and of upward motions in such a mechanism. Mode 2, corresponding to a simultaneous increase of SST and large-scale subsidence, mainly occurs over the Pacific and Indian oceans where SST is the warmest. This decoupling between the vertical motion and the SST can be explained by the seasonal monsoon circulation and/or the influence of Madden and Julian oscillation [*Bony et al.*, 1997]. Mode 3 is located over subtropical oceans and off the west coast of lands. In these regions the vertical dynamics changes are weak with regard to SST changes.

In the case of interannual variation (Figure 8), mode 1, which represents more than 40% of the total situations, largely dominates, except over Indonesia and the east Pacific Ocean. Mode 2 is also very representative (more than 35% of the total situations) and is largely present, except in central Pacific and Indian oceans. In these latter regions, mode 3 is dominant.

This method of characterizing the relative change of vertical motion with respect to SST is derived from a study by *Bony et al.* [1997]. The two studies show similar results [see of *Bony et al.*, Figure 8, 1997]. However, the present approach uses the indicator λ_2, directly obtained from observations, whereas Bony et al. use the vertical velocity at 500 hPa computed by a general circulation model. The good agreement shows the coherence between the vertical velocity from a model and the vertical dynamics indicator as inferred from TOVS-3I.

4.2. Relationship Between Vertical Distribution of Water Vapor, SST, and Vertical Dynamics

Using (3) and (4), it follows that

$$\frac{dw_{\text{par}}}{w_{\text{par}}} = a d\text{SST} - b_{\text{par}}(\lambda)\,\frac{d\lambda}{\lambda + 1}, \qquad (6)$$

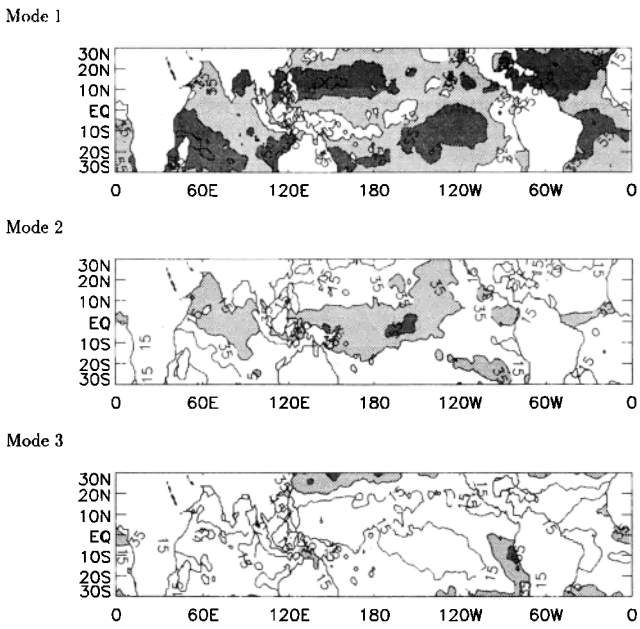

Figure 7. Geographical distribution of occurrence (in percent) for the three different modes of I_c (see text) for the seasonal variation. Contour interval is 20%, and values between 15 and 35% (over 35%) are shaded in light (dark) gray.

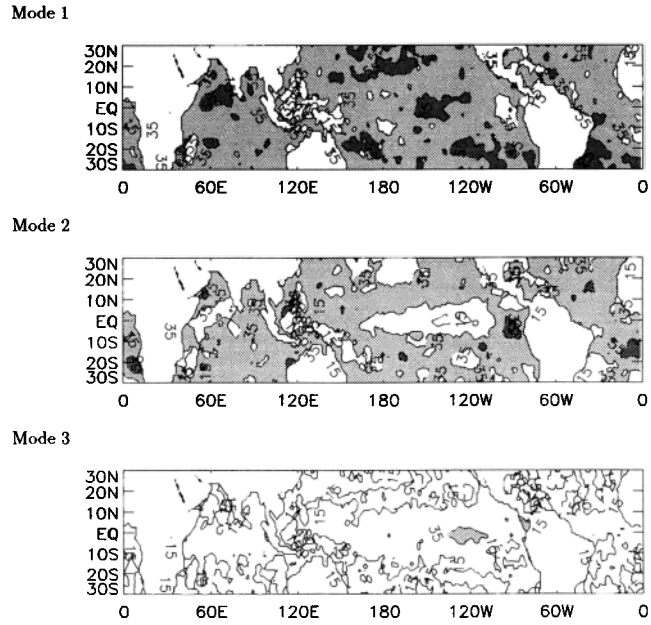

Figure 8. Same as Figure 7 but for interannual variations.

where $b_{\text{par}}(\lambda)$ is a positive function increasing with λ, in the interval of λ considered here, and depending on p_{sup} and p_{inf}. In particular, for the 700- to 500-hPa layer the latter equation becomes

$$\frac{1}{w_{700\text{–}500}}\,\frac{\Delta w_{700\text{–}500}}{\Delta\text{SST}} = a - b_{700\text{–}500}(\lambda_2) I_d, \qquad (7)$$

where $I_d = I_c/(\lambda_2 + 1)$, and thus it is the index of relative change of λ_2 with respect to SST. Equation (7) expresses the relationship between the variations of the water vapor content in the 700- to 500-hPa layer, on the one hand, and the large-scale vertical dynamics index, on the other hand, with the SST. Since $b_{700\text{–}500}$ slightly increases from 2 to 2.5 when λ increases from 3 to 4, $1/w_{700\text{–}500} \times \Delta w_{700\text{–}500}/\Delta\text{SST}$ is positive (negative) when I_d is smaller than a/b, notably for mode 1 (greater than a/b, especially for mode 2).

Figures 9 and 10 show the observed relative change of w_{par} with SST for the three layers according to I_d for the seasonal (Figure 9) and the interannual variations (Figure 10). In addition, the function $a + b_{\text{par}} I_d$ has been plotted with b_{par} values of 0.2 for the surface to 700-hPa layer and of 1.5 for the 500- to 300-hPa and 700- to 500-hPa layers. The values of each b_{par} have been chosen to best fit the observations. Note that a value of $b_{700\text{–}500}$ equal to 1.5 corresponds to a realistic value of λ_2 around 2.5. It shows that (7) is approximately verified in the 700- to 500-hPa layer both for the seasonal and the interannual variation. Moreover, the relative change of water vapor with respect to SST in the 500- to 300-hPa layer decreases with increasing I_d with the same gradient as in the 700–500 layer. The largest standard deviations around this average behavior found for the 500- to 300-hPa layer suggest the influence of other factors in the monthly distribution of water vapor in the upper troposphere, such as horizontal advection. *Sherwood* [1996] has shown that horizontal and vertical advection are of nearly the same magnitude above 500 hPa and that any potential source of water vapor is negligible. In the surface- to 700-hPa layer the rate of change of the water vapor content with respect to SST does not vary too much with I_d.

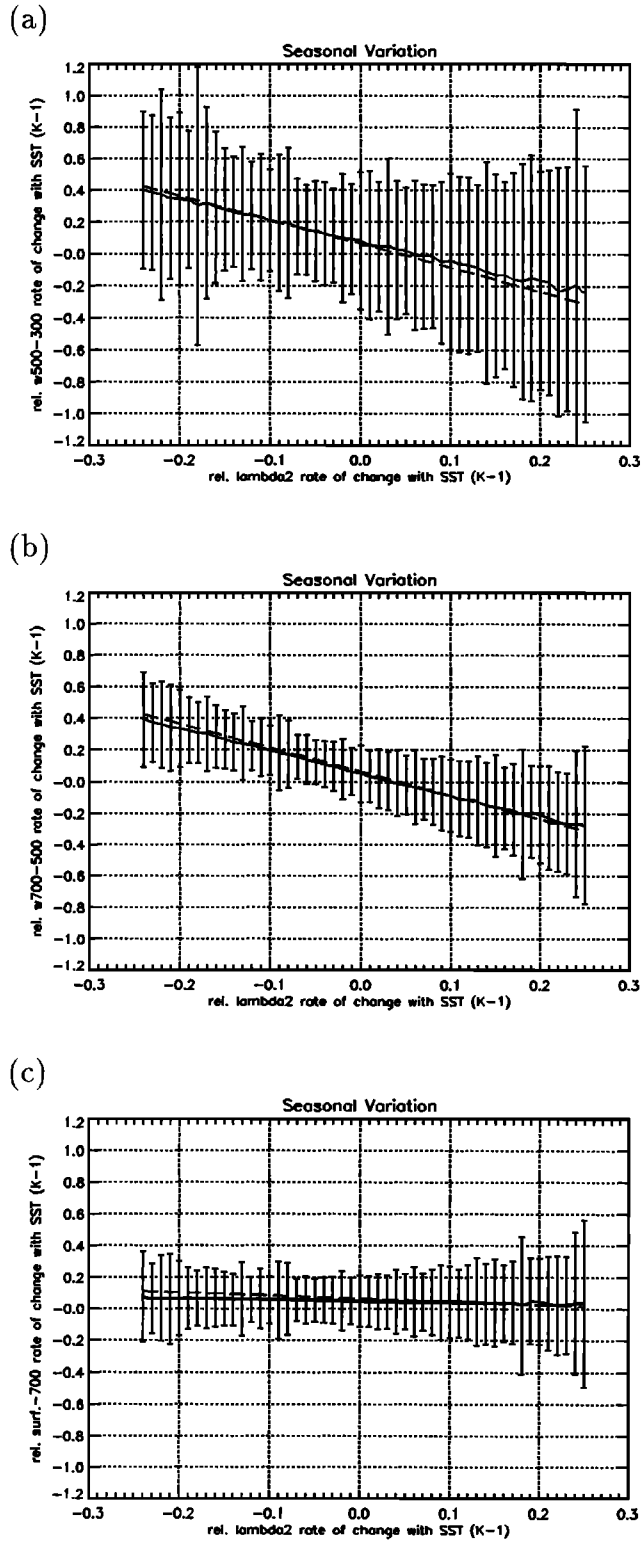

Figure 9. Seasonal variation of $1/w_{\text{var}} \times \Delta w_{\text{par}}/\Delta\text{SST}$, the relative change of w_{par} with SST, according to I_d, and the relative change of λ_2 with SST (a) in the 500- to 300-hPa layer, (b) in the 700- to 500-hPa layer, and (c) in the surface- to 700-hPa layer. In addition, the function $a + b_{\text{var}} I_d$ has been plotted with b_{par} values of 0.2 for the surface- to 700-hPa layer and of 1.5 for the 500- to 300-hPa, and 700- to 500-hPa layers.

It follows that the role of the vertical dynamics on the water vapor content in the lower troposphere is negligible with respect to that of the SST. On the contrary, in the upper layers the vertical dynamics make an important contribution to the distribution of the water vapor. For instance, with a positive SST perturbation of 1 K a 10% enhancement of upward motion (more precisely a 10% of λ_2 diminution) leads to a 20%

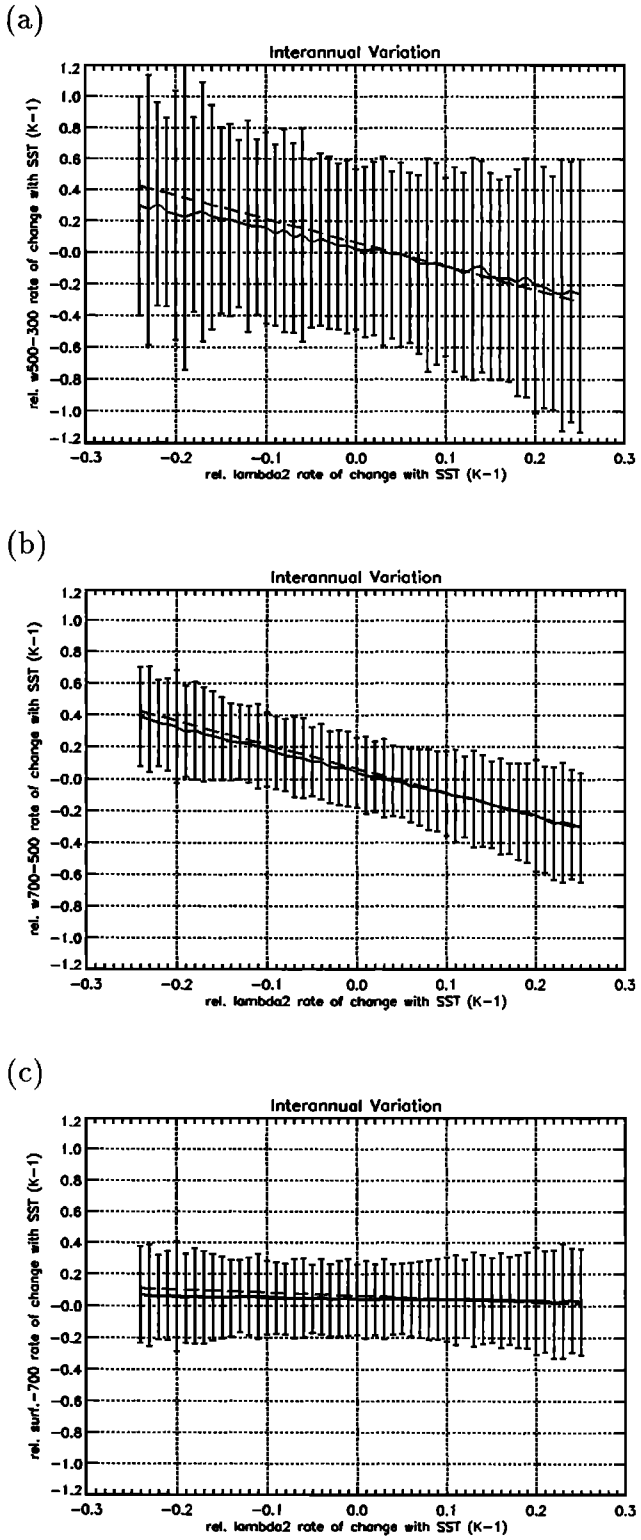

Figure 10. Same as Figure 9 but for interannual variations.

increase of the water vapor content in the 700- to 500-hPa and in the 500- to 300-hPa layers. In contrast, for the same positive SST perturbation a 10% diminution of upward motions leads to a 10% decrease of the water vapor content in the same layers.

5. Conclusion

We have presented an original method showing the vertical variation of the dynamical influences in the distribution of the water vapor. For each layer of the troposphere (surface–700 hPa, 700–500 hPa, and 500–300 hPa) we have computed a parameter (λ), ratio of the atmosphere scale height to the specific humidity scale height. The value λ represents the relative contribution of the dynamic influence to the water vapor content. We show that the vertical variation of λ expresses the diversity of dynamic contributions according to tropospheric layers. The study has led us to identify, among the different computed λ, a more specific vertical dynamic indicator, corresponding to the 700- to 500-hPa layer. Using this latter parameter, we have examined the link between SST and vertical dynamics and its impact on the water vapor vertical distribution. While the link between surface temperature and water vapor described by the Clausius-Clapeyron relationship is generally verified, vertical dynamics also contribute significantly to water vapor content variations, particularly in the middle and the upper troposphere.

The analysis of the geographical distribution of seasonal and interannual variability shows that in the lower troposphere a SST increase can lead to a water vapor content increase, independently of the dynamical regime (subsidence or large-scale rising motion). However, water vapor contents in the middle and the upper troposphere do not systematically vary with SST but depend concurrently on dynamics and thermodynamics. The results show that the rate of change of water vapor content in the 700- to 500- and 500- to 300-hPa layers with respect to SST increases with decreasing rate of change of λ_2 with respect to SST, that is, with increasing rate of change of upward vertical dynamics with respect to SST. A study similar to that done in section 4.2 could be done with the vertical velocity at 500 hPa from an atmospheric general circulation model in order to test its large-scale motions within the tropics.

Presently limited in time (31 months), this global analysis of the vertical distribution of water vapor content will be extended to the almost 20-year observations (1979 to now) of NOAA satellites. It will permit the extension of this work, in particular, to one of the most important El Niño event of the century (1982–1983). Moreover, a more complete and unambiguous understanding of the link between surface temperature, water vapor distribution, and vertical dynamics implies a strong coupling between climate modeling and observation.

Acknowledgments. The satellite data were provided to us within the framework of the NOAA/NASA Pathfinder Program. This work has been supported by CNRS and CNES and by the Commission of the European Community, contracts EV5V-CT92-0131 and EV5V-CT94-0441. Also this work has been supported by grants from IBM. Computations have been performed at IDRIS (Institut du Developpement et des Ressources en Informatique Scientifique) of CNRS.

References

Achard, V., Trois problèmes clés de l'analyse 3D de la structure thermodynamique de l'atmosphère: Mesure du contenu en ozone, classification des masses d'air, modélisation "hyper" rapide du transfert radiatif, Ph.D. thesis, Univ. Paris VII, Paris, 1991.

Bony, S., K.-M. Lau, and Y. C. Sud, Sea surface temperature and large-scale circulation influences on tropical greenhouse effect and cloud radiative forcing, *J. Clim.*, *10*, 2055–2077, 1997.

Cess, R. D., et al., Intercomparison and interpretation of climate feedback processes in 19 atmospheric general circulation models, *J. Geophys. Res.*, *95*, 16,601–16,615, 1990.

Chaboureau, J.-P., A. Chédin, and N. A. Scott, Remote sensing of the vertical distribution of atmospheric water vapor from the TOVS observations: Method and validation, *J. Geophys. Res.*, *103*, 8743–8752, 1998.

Chahine, M. T., Observation of local cloud and moisture feedbacks over high ocean and desert surface temperatures, *J. Geophys. Res.*, *100*, 8919–8927, 1995.

Chédin, A., and N. A. Scott, Improved Initialization Inversion procedure ("3I"), in *Proceedings of the First TOVS Study Conference*, Igls, Austria, edited by P. Menzel, pp. 14–79, Coop. Inst. for Meteorol. Satell. Stud., Igls, Austria, 1984.

Chédin, A., N. A. Scott, C. Wahiche, and P. Moulinier, The Improved Initialization Inversion method: A high-resolution physical method for temperature retrievals from the TIROS-N series, *J. Clim. Appl. Meteorol.*, *24*, 124–143, 1985.

Chevallier, F., F. Chéruy, N. A. Scott, and A. Chédin, A neural network approach for a fast and accurate computation of longwave radiative budget, *J. Appl. Meteorol.*, in press, 1998.

Escobar-Munoz, J., Base de données pour la restitution de paramètres atmosphériques à l'échelle globale: Etude de l'inversion par résaux de neurones des données des sondeurs verticaux atmsophériques satellitaires présents et à venir, Ph.D. thesis, Univ. Paris VII, Paris, 1993.

Fu, R., A. D. Del Genio, W. B. Rossow, and W. T. Liu, Cirrus-cloud thermostat for tropical sea surface temperatures tested using satellite data, *Nature*, *358*, 394–397, 1992.

Gadgil, S., P. V. Joseph, and N. V. Joshi, Ocean-atmosphere coupling over monsoon regions, *Nature*, *312*, 141–143, 1984.

Graham, N. E., and T. P. Barnett, Sea surface temperature, surface wind divergence and convection over tropical oceans, *Science*, *238*, 657–659, 1987.

Hallberg, R., and A. K. Inamdar, Observations of seasonal variations in atmospheric greenhouse trapping and its enhancement at high sea surface temperature, *J. Clim.*, *6*, 920–930, 1993.

Inamdar, A. K., and V. Ramanathan, Physics of the greenhouse effect and convection in warm oceans, *J. Clim.*, *7*, 715–731, 1994.

Lindzen, R. S., Some coolness concerning global warming, *Bull. Am. Meteorol. Soc.*, *71*, 288–299, 1990.

Peixoto, J., and A. Oort, *Physics of Climate*, 520 pp., Am. Inst. of Phys., Greenbelt, Md., 1992.

Prabhakara, C., G. Dalu, R. C. Lo, and N. R. Nath, Remote sensing of seasonal distribution of precipitable water over the oceans and the inference of boundary-layer structure, *Mon. Weather Rev.*, *107*, 1388–1401, 1979.

Ramanathan, V., and W. Collins, Thermodynamic regulation of ocean warming by cirrus clouds deduced from observations of the 1987 El Niño, *Nature*, *351*, 27–32, 1991.

Raval, A., and V. Ramanathan, Observational determination of the greenhouse effect, *Nature*, *342*, 758–761, 1989.

Rind, D., E. W. Chiou, W. P. Chu, J. C. Larsen, S. Oltmans, M. P. McCormick, and L. R. McMaster, Positive water vapor feedback in climate models confirmed by satellite data, *Nature*, *349*, 500–503, 1991.

Sherwood, S. C., Maintenance of the free-tropospheric tropical water vapor distribution, I, Clear regime budget, *J. Clim.*, *9*, 2903–2918, 1996.

Smith, W. L., Note on the relationship between total precipitable water and surface dew point, *J. Appl. Meteorol.*, *3*, 726–727, 1966.

Smith, W. L., H. M. Woolf, C. M. Hayden, D. Q. Wark, and L. M. McMillin, The TIROS-N operational vertical sounder, *Bull. Am. Meteorol. Soc.*, *60*, 1177–1187, 1979.

Stephens, G. L., On the relationship between water vapor over the oceans and sea surface temperature, *J. Clim.*, *3*, 634–645, 1990.

Stephens, G. L., and T. J. Greenwald, The Earth's radiation budget and its relation to atmospheric hydrology, 1, Observations of the clear sky greenhouse effect, *J. Geophys. Res.*, *96*, 15,311–15,324, 1991.

Stubenrauch, C. J., N. A. Scott, and A. Chédin, Cloud field identifi-

cation for Earth radiation budget studies, I, Cloud field classification using HIRS/MSU sounder measurements, *J. Appl. Meteorol.*, *35*, 416–427, 1996.

Waliser, D. E., and N. E. Graham, Convective cloud systems and warm-pool sea surface temperatures: Coupled interactions and self-regulation, *J. Geophys. Res.*, *98*, 12,881–12,893, 1993.

Waliser, D. E., N. E. Graham, and C. Gautier, Comparison of the highly reflective cloud and outgoing longwave radiation datasets for use in estimating tropical deep convection, *J. Clim.*, *6*, 331–353, 1993.

Wallace, J. M., Effect of deep convection on the regulation of tropical sea surface temperature, *Nature*, *357*, 230–231, 1992.

J.-P. Chaboureau, Department of Meteorology, University of Reading, P.O. Box 243, Reading RG6 6BB, England, UK. (j-p.chaboureau@reading.ac.uk)

A. Chedin and N. A. Scott, Laboratoire de Météorologie Dynamique du CNRS, École Polytechnique, Palaiseau, France. (e-mail: chedin@ara01.polytechnique.fr; scott@ara01.polytechnique.fr)

(Received January 6, 1998; revised June 5, 1998;
accepted June 5, 1998.)